AIP Journal of Applied Physics

# Exchange bias effect in BiFeO3-NiO nanocomposite

Kaushik Chakrabarti, Babusona Sarkar, Vishal Dev Ashok, Kajari Das, Sheli Sinha Chaudhuri, Amitava Mitra, and S. K. De

Citation: Journal of Applied Physics **115**, 013906 (2014); doi: 10.1063/1.4861140
View online: http://dx.doi.org/10.1063/1.4861140
View Table of Contents: http://scitation.aip.org/content/aip/journal/jap/115/1?ver=pdfcov
Published by the AIP Publishing

# Exchange bias effect in $BiFeO_3$-NiO nanocomposite

Kaushik Chakrabarti,[1] Babusona Sarkar,[1] Vishal Dev Ashok,[1] Kajari Das,[1] Sheli Sinha Chaudhuri,[2] Amitava Mitra,[3] and S. K. De[1,a)]
[1]*Department of Materials Science, Indian Association For the Cultivation of Science, Jadavpur, Kolkata 700032, India*
[2]*Department of Electronics and Telecommunication Engineering, Jadavpur University, Jadavpur, Kolkata 700032, India*
[3]*Material Science and Technology Division, CSIR-National Metallurgical Laboratory, Jamshedpur 7, India*

(Received 25 October 2013; accepted 16 December 2013; published online 7 January 2014)

Ferromagnetic $BiFeO_3$ nanocrystals of average size 11 nm were used to form nanocomposites (x)$BiFeO_3$/(100 − x)NiO, x = 0, 20, 40, 50, 60, 80, and 100 by simple solvothermal process. The ferromagnetic $BiFeO_3$ nanocrystals embedded in antiferromagnetic NiO nanostructures were confirmed from X-ray diffraction and transmission electron microscope studies. The modification of cycloidal spin structure of bulk $BiFeO_3$ owing to reduction in particle size compared to its spin spiral wavelength (62 nm) results in ferromagnetic ordering in pure $BiFeO_3$ nanocrystals. High Neel temperature ($T_N$) of NiO leads to significant exchange bias effect across the $BiFeO_3$/NiO interface at room temperature. A maximum exchange bias field of 123.5 Oe at 300 K for x = 50 after field cooling at 7 kOe has been observed. The exchange bias coupling causes an enhancement of coercivity up to 235 Oe at 300 K. The observed exchange bias effect originates from the exchange coupling between the surface uncompensated spins of $BiFeO_3$ nanocrystals and NiO nanostructures. © *2014 AIP Publishing LLC*. [http://dx.doi.org/10.1063/1.4861140]

## I. INTRODUCTION

Nanocomposite consisting of at least one material in nanometer scale is a very attractive and fascinating class of system to tune the physical properties of constituent components. The synergetic effect leads to unusual phenomenon not originally observed in individual component. Nanocomposite constitutes interface along the boundary of each material providing an effective medium based on interfacial interaction. The ferromagnetic (FM)/antiferromagnetic (AFM) interface results in exchange bias (EB) effect, which was first observed by Meiklejohn and Bean in 1956. This novel phenomenon opens up a new branch of research in magnetic materials.[1] Structural discontinuity and mismatch of spin alignment across the interface give rise to complex magnetic exchange interaction at the interface.[2,3] The EB effect has enormous applications in spintronics and high density data storage devices.[4–7] The EB phenomenon arises from the FM/AFM interface as it is cool down from above the Neel Temperature ($T_N$) of the AFM in the presence of an external magnetic field.[2] The ordered AFM spins couple with the FM spins at the interface below $T_N$ in the presence of external magnetic field, which results in unidirectional exchange anisotropy. This additional anisotropy manifests in the form of shift in the hysteresis curve along the magnetic field axis. The magnitude of shift along the magnetic field axis actually quantifies exchange bias field ($H_{EB}$), which mainly depends on the direction and magnitude of the cooling magnetic field, volume or thickness of both FM and AFM materials, anisotropy energy of the AFM, and the nature of interaction between the FM and AFM spins at the interface.[8,9] Fabrication of interface in layered FM and AFM materials is generally done by costly equipment and complicated procedure.[10,11] Interface can be generated in core (FM or AFM)-shell (AFM or FM) nanostructures through complex chemical process.[12] The formation of composite is an efficient way for fabricating interface by dispersing one magnetic phase into another leading to enhanced proximity effect across the interface.[13,14] The composite in the nanoscale regime creates a larger number of interfaces due to higher number of surfaces thereby enhancing the EB effect.[15] The surface spin structure of nanoscale AFM and FM materials plays an important role in controlling the interfacial exchange strength, which ultimately affects the EB effect.

A suitable combination of FM and AFM materials is necessary to generate significant amount of $H_{EB}$ at room temperature. Bismuth ferrite ($BiFeO_3$) and nickel oxide (NiO) are most interesting systems due to their novel magnetic properties. Simple NaCl type cubic structure and high $T_N$ (~523 K) of bulk NiO indicate a possibility of exchange coupling at room temperature. The spins in NiO are ferromagnetically coupled within the (111) planes, whereas the spins of alternating (111) planes are coupled antiferromagnetically.[16] High magnetic anisotropies both perpendicular and parallel to (111) planes ($K_\perp = 3.3 \times 10^5$ J/m$^3$ and $K_\parallel = 33$ J/m$^3$, respectively) fulfil one of the criteria for EB effect.[16] Earlier studies show that NiO nanostructures exhibit large coercive fields and high susceptibility at low temperature due to surface anisotropy.[17–19] The appearance of EB effect in NiO nanostructures is interpreted in terms of magnetic core-shell model, where the core acts as AFM and the shell behaves as uncompensated surface spins.[20]

The multiferroic oxide $BiFeO_3$ (BFO) is a basic G-type antiferromagnetic material having rhombohedral R3C symmetry with $T_N \sim 643$ K and ferroelectric curie temperature ($T_{FE}$) ~ 1103 K indicating a possibility for multifunctional

a)Electronic mail: msskd@iacs.res.in

 

applications.[21,22] The modulated spiral spin structure of bulk BFO has a wavelength of 62 nm.[23–26] BFO nanocrystals or nanowires having dimension comparable or smaller than its spin spiral wavelength reveal weak ferromagnetic behavior due to uncompensated surface spins and partial destruction of spin spiral structure.[27,28] There were several reports on EB effect in BFO thin films where BFO had been used as an AFM material.[29–31] Unusual EB effect has also been observed in pure and doped BFO nanocrystals due to two dimensional dilute AFM shell and AFM core.[32,33] The observation of EB phenomenon using BFO as FM material is very scarce. However, the appearance of strong ferromagnetic phase in BFO nanocrystals signifies the novelty in EB effect.

The most attractive feature of both BFO and NiO is the observation of EB effect due to spiral spin structure and uncompensated surface spins. The coupling among the uncompensated surface spins at the interface of composite may lead to prominent EB effect at room temperature. These features triggered us to synthesize BFO/NiO nanocomposite and study the magnetic property of their interface at room temperature. In this work, we present a detailed temperature and field dependent magnetization and EB effect specially at room temperature by varying the compositional ratio of FM component in nanocomposites. Incorporation of BFO nanocrystals of average size around 11 nm into the NiO matrix gives a reasonable high EB value of 123.5 Oe at 300 K. A reasonable vertical shift in positive direction of 0.095 emu/gm at 300 K has also been observed.

## II. EXPERIMENT

All the chemicals and solvents were of analytical grade and used without further purification. Nanocomposite $(x)BiFeO_3/(100 - x)NiO$ with $x = 0$, 20, 40, 50, 60, 80, and 100 were synthesized via two step solvothermal process: (i) synthesis of pure $BiFeO_3$ nanoparticles and (ii) dispersing the as prepared $BiFeO_3$ nanoparticles into NiO matrix. The precursor solution used in synthesizing pure $BiFeO_3$ nanoparticles was prepared by mixing $Bi(NO_3)_3{\cdot}5H_2O$ and $Fe(NO_3)_3{\cdot}9H_2O$ with 1:1.2 molar ratio into a mixed solvent of deionized (DI) water and ethylenediamine (4:1) under constant magnetic stirring for 3 h. An aqueous solution of 0.3N NaOH was prepared separately and added to the above precursor solution. The resultant solution was further stirred for another 2 h and was transferred to teflon lined steel chamber filled to 80% of its volume. The chamber was then closed and placed inside a preheated box furnace at 180 °C for 20 h. The crystalline brownish powder obtained after the reaction was collected by centrifugation and thorough washing with DI water and ethanol. Finally, the sample was dried under vacuum condition.

$(x)BiFeO_3/(100 - x)NiO$ nanocomposites were prepared by dispersing as synthesized $BiFeO_3$ nanoparticles in appropriate amounts into the precursor aqueous solution of $Ni(CH_3COO)_2{\cdot}H_2O$. After 1.5 h of dispersion, separately prepared aqueous solution of 4 mM $CH_4N_2O$ (Urea) was added to the precursor solution. The resultant solution was then transferred to teflon coated steel chamber filled until 80% of its volume. The chamber was then closed and placed inside a preheated box furnace at 180 °C for 16 h. Crystalline blackish-brown powders were collected by centrifugation and thorough washing with DI water and ethanol at the completion of the reaction. The product was finally dried under vacuum condition for 24 h.

The crystalline phases of the samples were determined by high-resolution X'Pert Pro Panalytical X-Ray diffractometer with Cu Kα radiation ($\lambda = 1.54$ Å). Microstructural analysis was performed by transmission electron microscope (TEM) and high resolution transmission electron microscope (HRTEM) using JEOL 2010 instrument. Temperature dependent magnetization-magnetic field (M-H) measurements for all the samples were carried out using Vibrating Sample Magnetometer (Lakeshore 7404). Differential scanning calorimetry (DSC, Perkin Elmer) of the sample was carried out to study the magnetic transition temperature.

## III. RESULTS AND DISCUSSION

Individual phases of nanocomposite were identified by X-ray diffraction. Figure 1 shows the room temperature X-ray diffraction patterns for $(x)BiFeO_3/(100 - x)NiO$ ($x = 0$, 20, 40, 50, 60, 80, and 100). The diffraction peaks of pure NiO ($x = 0$) exhibit (111) and (200) characteristic peaks of NaCl type crystalline NiO (matched to JCPDS File No. 78 0429). The diffraction pattern for pure BFO ($x = 100$) shows all peaks corresponding to the reflections from (012), (104), (110), (006), (202), (024), (116), and (018) planes of rhombohedral $BiFeO_3$ (JCPDS File No. 71 2494) with space group R3c. The evolution and presence of characteristic peaks of NiO and $BiFeO_3$ confirm the formation of nanocomposite.

Figure 2 shows the TEM images of the $(x)BiFeO_3/(100 - x)NiO$ nanocomposites with $x = 0$, 50, and 100. Figure 2(a) gives the network like structures of the pure NiO ($x = 0$). The parallel fringes as seen in HRTEM image in Fig. 2(b) give the lattice spacing of about 0.21 nm corresponding to (200) plane of cubic NiO phase. The FFT pattern shown in the inset of Fig. 2(b) also indicates the same plane of NiO. The cross fringes in the HRTEM image and diffused FFT pattern appear due to the network like structure of NiO. Figure 2(c) shows the TEM image of the sample for $x = 100$,

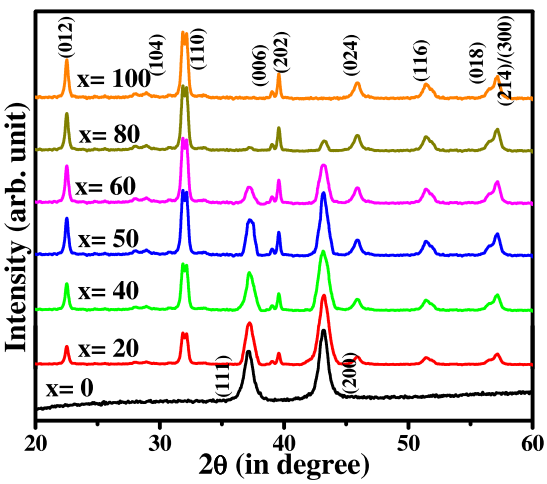


FIG. 1. Room temperature X-ray diffraction for $(x)BiFeO_3/(100 - x)NiO$, $x = 0$, 20, 40, 50, 60, 80, and 100.

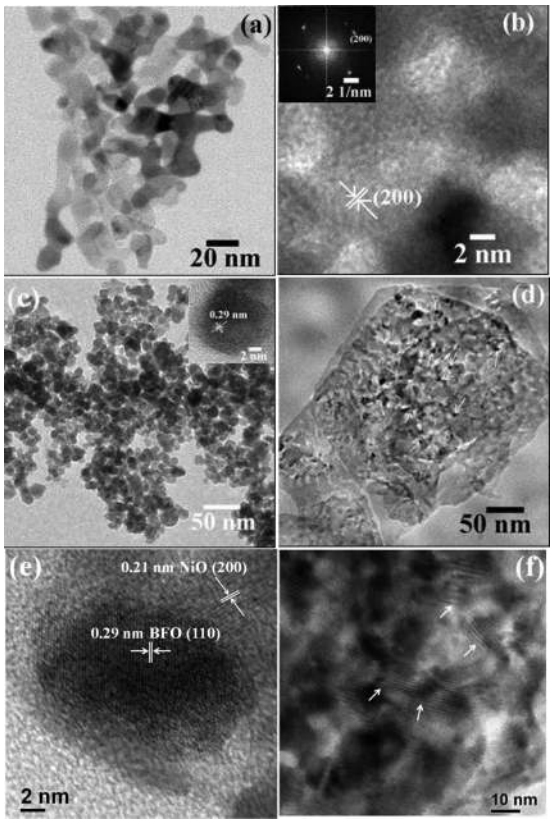


FIG. 2. TEM and HRTEM images of (x)$BiFeO_3$/(100 − x)NiO (a) low resolution image of x = 0, (b) high resolution image of x = 0 inset shows FFT patterns, (c) low resolution image of x = 100, inset shows high resolution image, (d) low resolution image of x = 50, (e) high resolution image of x = 50, and (f) locations of moire like patterns for x = 50.

i.e., pure BFO nanocrystals of average size ~11 nm. The calculated lattice spacing of 0.29 nm from HRTEM image of BFO nanocrystal shown in the inset of Fig. 2(c) confirms the (110) plane of $BiFeO_3$. Figure 2(d) reveals the interface of the nanocomposite for x = 50. The white arrows highlight the BFO nanocrystals embedded in the NiO matrix. The HRTEM image for x = 50 (Fig. 2(e)) presents a clear contrast in boundary showing the phase segregation of BFO with the plane (110) observed on the inside and NiO plane corresponding to (200) seen on the outside. A high concentration of Moire like patterns as indicated by white arrows in Fig. 2(f) is also observed, which we believe to have formed by the frustrated growth of NiO on BFO nanoparticles. This is similar to the amorphous structural defects arising due to breaking of bonds and chemical intermixing across the interface as observed in earlier studies.[34–36] This may also be supported by the presence of branched and spherical or round edges of NiO particle, which shows similar features of a non equilibrium growth (e.g., Laplacian growth).

To understand the formation of the particular network structure of NiO, a growth mechanism from aggregation, i.e., Ostwald step rule[37] in the solution can be summarized as follows. In the experimental solution of urea and $Ni(CH_3COO)_2$ (pH ~ 8), hexaaquo $Ni^{2+}$ ion $[Ni(H_2O)_6{}^{2+}]$ predominates than the other ions. The formation and edge-on condensation of tetramer from these ions at the high temperature nucleate the α-$Ni(OH)_2$ single layer structure.[38] Therefore, the initial precipitation provides numerous $Ni(OH)_2$ nucleation centers. Due to the anisotropy of α-$Ni(OH)_2$ crystals, the growing point of each crystal is located along certain directions, so network like structures were formed. As the reaction proceeds, the α-$Ni(OH)_2$ phase was completely transformed to the pure phase NiO. For the case of the BFO/NiO composites, the BFO nanocrystals present in the experimental solution were embedded in the α-$Ni(OH)_2$ layer structures during nucleation. So network like (x)$BiFeO_3$/(100 − x)NiO nanostructures were finally obtained.

Figure 3 shows room temperature (T = 300 K) 7 kOe field cooled (FC) magnetization-magnetic field (M-H) curves for x = 0 and 100, respectively. The hysteresis curve (FC M-H) as in Fig. 3(a) for x = 0 (pure NiO) shows basic antiferromagnetic behavior with loop not saturating at 11 kOe of applied magnetic field. A shift of 30 Oe along the negative field axis at T = 300 K is shown in the lower inset of Fig. 3(a). The observed hysteresis loop shift is defined as EB. Mathematically, the EB field ($H_{EB}$) and coercivity ($H_C$) for shifted hysteresis loop can be expressed as $H_{EB} = -(H_{C1} + H_{C2})/2$ and $H_C = (H_{C1} - H_{C2})/2$. $H_{C1}$ and $H_{C2}$ are points where the hysteresis loop intersect magnetic field axis. A shift of 30 Oe along the magnetic field axis for x = 0 may be attributed to the exchange coupling between uncompensated surface spins of NiO nanostructure and the spins of AFM core.[20] The DSC result in the temperature range of 300 K to 550 K for pure NiO is shown in the upper inset of Fig. 3(a). A kink like anomaly is observed at around 400 K of temperature indicating a second order magnetic phase transition for pure NiO.[39] The Neel temperature ($T_N$) for pure NiO as determined from DSC is around 400 K, which is much lower than its bulk value (523 K).[16] The reduction in size from

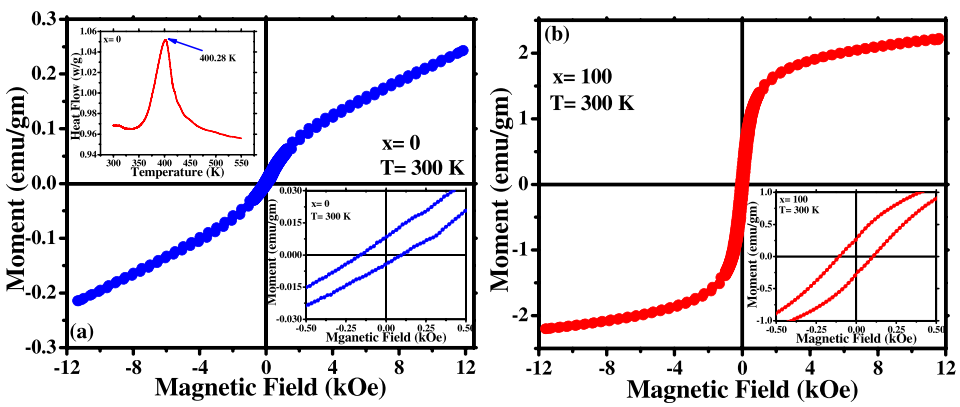


FIG. 3. Field cooled (7 kOe) M-H curves for (x)$BiFeO_3$/(100 − x)NiO (a) x = 0 (upper and lower insets show the differential scanning calorimetry thermogram and magnified M-H loop, respectively) and (b) x = 100 (inset shows the magnified M-H curve).

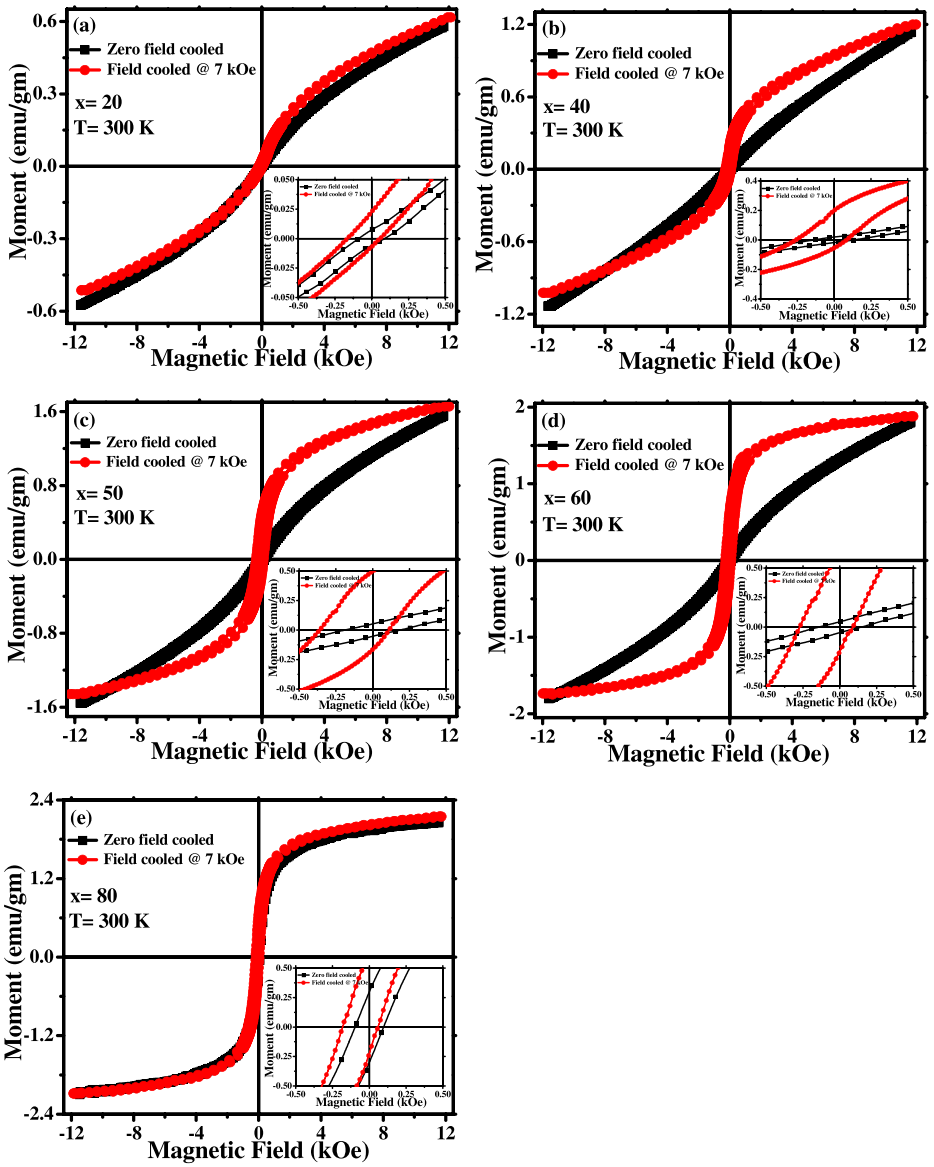


FIG. 4. Zero field cooled and 7 kOe field cooled M-H curves at T = 300 K for (x)$BiFeO_3$/(100 − x)NiO (a) x = 20, (b) x = 40, (c) x = 50, (d) x = 60, and (e) x = 80. Insets show the magnified M-H curves in the low magnetic field region for all samples.

bulk to nanoscale regime in NiO actually weakens the magnetic exchange interaction, which results in lowering of $T_N$.

The M-H curve for x = 100 as shown in Fig. 3(b) reveals ferromagnetic behavior without any loop shift (as shown in the inset of Fig. 3(b)) along the magnetic field axis. The observed ferromagnetic ordering in pure BFO nanocrystals mainly occurs due to reduction in particle size as compared to the wavelength (62 nm) of spiral modulated spin structure of bulk BFO.[27,28] The observed saturation magnetization ($M_S$) of 2.2 emu/gm at T = 300 K and H = 7 kOe is consistent with previous report predicting an increase in $M_S$ with decreasing size of BFO nanocrystals.[28] Almost saturating magnetization curve, finite coercive field, and increment in $M_S$ support the ferromagnetic phase in BFO nanocrystals. Size reduction leads to destruction of spin spiral structure favoring ferromagnetic alignment of spins. Ferromagnetism

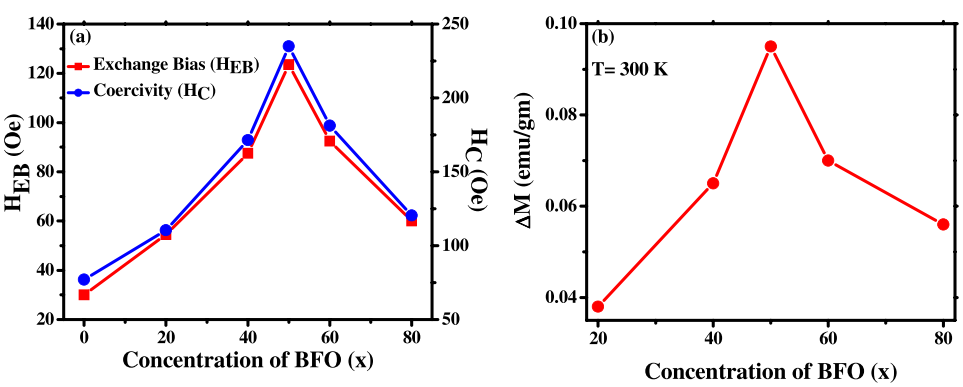


FIG. 5. Variation of (a) exchange bias field ($H_{EB}$) and coercivity ($H_C$) and (b) vertical shift (ΔM) with FM ratio (x) for (x)$BiFeO_3$/(100 − x)NiO at T = 300 K.

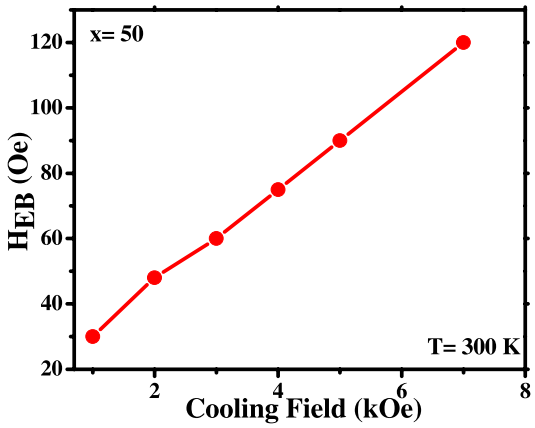


FIG. 6. Dependence of $H_{EB}$ with cooling field ($H_{cool}$) for (x)$BiFeO_3$/(100 − x)NiO, x = 50 at T = 300 K.

in BFO nanocrystals may also arise due to cation and oxygen vacancies.[40,41] The observed M-H curve is symmetric about the zero magnetic field axis as observed in the inset of Fig. 3(b). The EB effect in magnetic nanoparticles arises due to co-existence of different magnetic phases of core and surface spins. Single ferromagnetic phase in BFO nanocrystals thereby supports the absence of EB phenomenon.

Figure 4 shows zero field cooled and 7 kOe field cooled magnetic hysteresis curves for x = 20, 40, 50, 60, and 80 at 300 K of temperature. The insets of Figs. 4(a)–4(e) show magnified M-H curves in the low magnetic field region. The ZFC M-H curves for all compositions indicate symmetric nature about the magnetic field axis thereby revealing no EB effect. The FC process causes a negative horizontal shift along the magnetic field axis. When the samples are cooled down from $T_N$ of NiO in the presence of external magnetic field, the AFM spins residing next to the FM spins at the interface arrange along a specific direction. Below $T_N$, the AFM spins at the interface of FM/AFM structure exert microscopic torque on the FM spins thereby keeping them in their original direction. As a result of it, higher magnetic field is required to reverse FM spins causing a shift along the magnetic field axis.[9] In addition to the horizontal shift along the magnetic field axis, a positive vertical shift along the magnetization direction is also observed for all the samples. The vertical shift (ΔM) is defined as the difference in saturation magnetization between the hysteresis loop in FC and loop centered about the magnetization axis. The maximum value of ΔM is 0.095 emu/gm for x = 50. Positive vertical shift along the magnetization axis occurs if the number of magnetic moments in either FM or AFM layer at the interface remains uncompensated due to the proximity of the other layer.[42] The orientation of the magnetic moments can be parallel or antiparallel with respect to the FM layer thereby resulting in vertical shift of the hysteresis loop. The vertical shift in positive direction may arise due to direct exchange mechanism, whereas a shift in negative direction arises due to indirect exchange mechanism of the uncompensated magnetic moments.[43] A positive vertical shift (ΔM) for the present case reveals the existence of pinned uncompensated AFM (NiO) spins. These uncompensated spins are pinned along the field direction during the FC magnetization process thus cannot be rotated causing vertical shift.[44] Also, positive vertical shift suggests a direct exchange mechanism of these uncompensated pinned spins.[43] To gain further knowledge about the EB phenomenon for the present samples, we performed temperature and FM (BFO) ratio (x) dependent study of EB, coercivity ($H_C$), and ΔM in the following paragraphs.

Figure 5(a) shows the dependence of $H_{EB}$ and $H_C$ (calculated from the FC M-H) on the ferromagnetic (BFO) composition ratio x of the nanocomposites at 300 K of temperature. The value of $H_{EB}$ increases with x showing a maximum value of 123.5 Oe for x = 50 and decreases thereafter with further increase of x. The increase of $H_{EB}$ with x until x = 50 suggests a strong exchange coupling between BFO and NiO. For x < 50, the BFO nanocrystals are present in small quantity in NiO matrix in an isolated manner thereby increasing the exchange coupling with NiO.[45] Beyond x = 50, the BFO nanocrystals are coalesced to form isolated FM clusters thereby reducing the interfacial exchange coupling and results in decreasing $H_{EB}$. The inverse proportionality relationship between $H_{EB}$ and thickness of FM materials ($H_{EB} \propto 1/t_{FM}$) is a well established fact.[9] The formation of clusters from BFO nanocrystals beyond x = 50 results in increase of effective FM thickness thus decreasing the $H_{EB}$. $H_C$ also follows similar behavior as that of $H_{EB}$, increasing at first until x = 50 and decreasing thereafter. The relative phase component of FM and AFM in nanocomposite plays a vital role in determination of magnitude of EB and coercive fields.

Figure 5(b) shows the composition dependence of ΔM at T = 300 K. ΔM also follows similar pattern as observed in $H_{EB}$ and $H_C$. The decrease of ΔM beyond x = 50, which acts

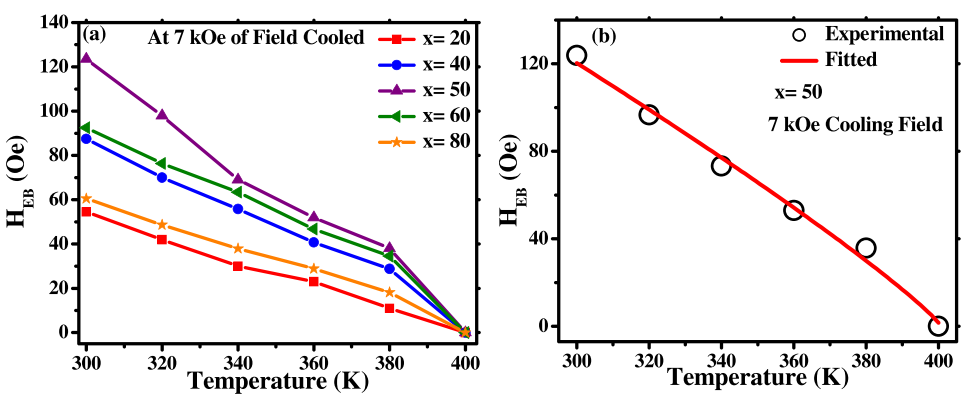


FIG. 7. Dependance of (a) $H_{EB}$ with temperature for (x)$BiFeO_3$/(100 − x) NiO, x = 20, 40, 50, 60, and 80 and (b) fitted $H_{EB}$ Vs temperature for (x)$BiFeO_3$/(100 − x)NiO, x = 50.

TABLE I. Parameters Neel temperature ($T_{N1}$, $T_{N2}$, and $T_{N3}$) and exponent ($\beta$, $\alpha$, and $\gamma$) obtained from fitting the $H_{EB}$, $\Delta M$, and $\Delta H_C$ with temperature for all compositions using Eqs. (1), (2), and (3).

| x | $T_{N1}$ (K) | $\beta$ | $T_{N2}$ (K) | $\alpha$ | $T_{N3}$ (K) | $\gamma$ |
|---|---|---|---|---|---|---|
| x = 20 | 400.73 ± 1.48 | 1.04 ± 0.04 | 400.51 ± 1.13 | 1.03 ± 0.03 | 400.26 ± 0.16 | 1.06 ± 0.02 |
| x = 40 | 400.03 ± 1.13 | 0.70 ± 0.06 | 400.21 ± 1.77 | 0.83 ± 0.07 | 400.12 ± 1.11 | 0.71 ± 0.06 |
| x = 50 | 400.77 ± 3.08 | 0.88 ± 0.09 | 400.31 ± 1.76 | 0.85 ± 0.06 | 400.04 ± 0.14 | 0.86 ± 0.01 |
| x = 60 | 400.01 ± 0.93 | 0.67 ± 0.05 | 400.01 ± 1.01 | 0.70 ± 0.05 | 400.10 ± 0.74 | 0.67 ± 0.04 |
| x = 80 | 400.24 ± 1.83 | 0.81 ± 0.06 | 405.88 ± 5.88 | 1.34 ± 0.33 | 400.18 ± 1.32 | 0.82 ± 0.05 |

as a percolation limit may be attributed to the formation of FM clusters from BFO nanocrystals. Thus, high proportion of FM phase decreases the value of $\Delta M$ beyond x = 50.[46]

Figure 6 shows the dependence of $H_{EB}$ on cooling field ($H_{cool}$) for x = 50 at 300 K of temperature. $H_{EB}$ increases with the increase of $H_{cool}$. The increase in cooling field leads to an enhancement of the alignment of FM moments along the preferential direction thereby reducing the effect of averaging of anisotropy due to randomness. The uncompensated AFM spins at the interface also align along the direction of the cooling field due to exchange coupling with FM spins. Thus, with the increase in cooling field more uncompensated AFM spins tried to align along the field direction thereby resulting in an increase of $H_{EB}$.[47]

Figure 7(a) shows the dependence of $H_{EB}$ on temperature for x = 20, 40, 50, 60, and 80. The EB effect is generally observed below $T_N$ in an FM/AFM interface with Curie temperature ($T_C$) > $T_N$ at high magnetic field. Thus, FM region attains almost saturation magnetization and hence there is no domain wall motion. The magnetic properties of FM component ideally remain independent of temperature. The main contribution of FM is to couple with the moments in AFM region leading to a thin ferromagnetic layer above $T_N$. The dynamics of AFM domain wall with temperature actually determines the temperature dependence of the parameters ($H_{EB}$, $H_C$, and $\Delta M$ as defined earlier) related to EB phenomenon. The thermal behavior of exchange bias parameters is generally derived from the temperature dependence of anisotropy and exchange stiffness constants of AFM. The domain wall energy is dependent on the anisotropy and stiffness constants and is an important quantity to describe the exchange parameters as a function of temperature. The domain wall energy approaches to zero at $T_N$ due to the disappearance of AFM order. The combination of AFM domain wall energy and interfacial energy stabilizes a magnetic state at a particular temperature. The minimization of total energy consisting of interfacial coupling and antiferromagnetic domain wall energy gives rise to a power law behavior in temperature.[48,49] The ratio (r) of interfacial exchange to domain wall energies determines the value of the exponent. The exchange anisotropy increases continuously for r >1 with decreasing temperature, which is consistent with the present observation as shown in Fig. 7(b). $H_{EB}$ becomes zero at $T_N$ of NiO as the spins participating in EB phenomenon loses its AFM ordering beyond $T_N$. The temperature dependence of $H_{EB}$ can be fitted by using the expression

$$H_{EB}(T) = A(1 - T/T_{N1})^{\beta}, \tag{1}$$

where A is a constant, $T_{N1}$ is the Neel temperature obtained from fitting, and $\beta$ is the exponent as shown in Fig. 7(b) for x = 50. The best fitted values for all compositions are shown in Table I. The values of $T_{N1}$ obtained from fitting closely resemble the experimental $T_N$ of NiO obtained from DSC.

Figure 8(a) shows the temperature dependence of $\Delta M$ for all the samples. $\Delta M$ also follows a similar trend as $H_{EB}$ with temperature. The drastic decrease of $\Delta M$ with increase of temperature suggests the weakening of exchange coupling at the interface due to the rise in temperature. The increase in temperature leads to increase in randomness of NiO spins thereby weakening the exchange coupling strength at the interface. $\Delta M$ also follows similar power law behavior with temperature. The expression used to fit $\Delta M$ with temperature is

$$\Delta M(T) = B(1 - T/T_{N2})^{\alpha}, \tag{2}$$

where B is a constant, $T_{N2}$ is the Neel temperature obtained from fitting, and $\alpha$ is the exponent as shown in Fig. 8(b) for x = 50. The best fitted values of the parameters are shown in

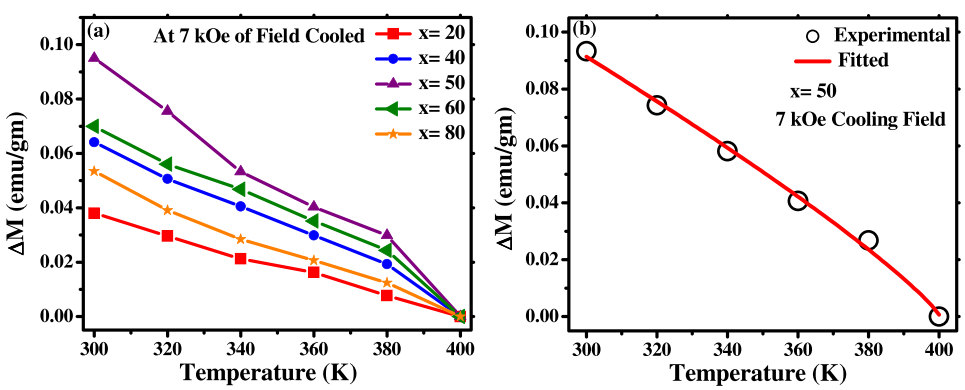


FIG. 8. Dependance of (a) $\Delta M$ with temperature for (x)$BiFeO_3$/(100 − x)NiO, x = 20, 40, 50, 60, and 80 and (b) fitted $\Delta M$ Vs temperature for (x)$BiFeO_3$/(100 − x)NiO, x = 50.

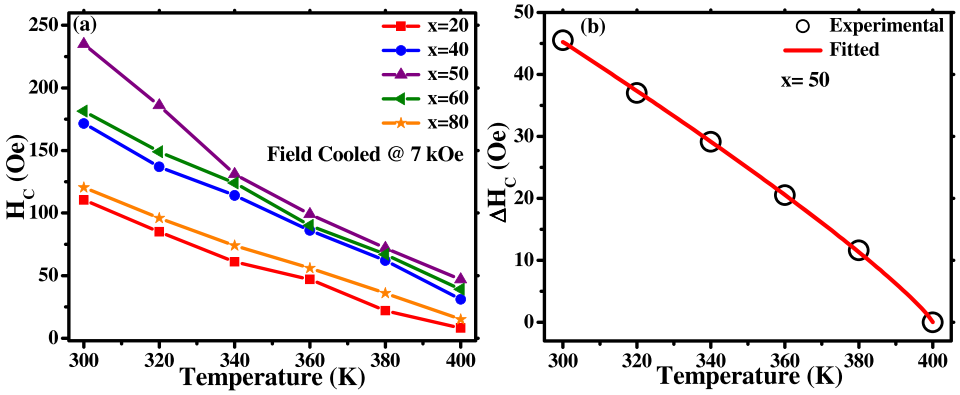


FIG. 9. Dependance of (a) $H_C$ with temperature for (x)$BiFeO_3$/(100 − x) NiO, x = 20, 40, 50, 60, and 80 and (b) fitted $H_C$ Vs temperature for (x)$BiFeO_3$/(100 − x)NiO, x = 50.

Table I. The estimated values of $T_{N2}$ from the fitting are very close to the actual $T_N$ of pure NiO derived from DSC result.

Figure 9(a) shows the variation of $H_C$ with temperature for x = 20, 40, 50, 60, and 80. The values of $H_C$ are calculated from field cooled M-H curves. A decrease in $H_C$ with increase in temperature is due to the fluctuation of spins and reduction in the exchange coupling between BFO and NiO. The magnitude of $H_C$ ($H_C$(FC)) in field cooled process is larger than the $H_C$ ($H_C$(ZFC)) in zero-field cooled process. The enhancement in $H_C$ may be attributed to the additional unidirectional anisotropy due to the exchange coupling between BFO and NiO at their interface. This increment in $H_C$, $\Delta H_C = H_C(FC) - H_C(ZFC)$ becomes 0 at the $T_N$ of NiO. Hence, the temperature dependence of $\Delta H_C$ is fitted using the following power law:

$$\Delta H_C = C(1 - T/T_{N3})^{\gamma}, \tag{3}$$

where C is a constant, $T_{N3}$ is the Neel temperature of NiO obtained from fitting, and $\gamma$ is the exponent as shown in Fig. 9(b) for x = 50. The best fitted value of the parameters is shown in Table I. The obtained value of $T_{N3}$ closely resembles the $T_N$ for NiO obtained previously from DSC result. The power law behavior to describe the temperature variation of exchange parameters has also been observed in FM and AFM heterostructure.[50–52]

The dependence of $H_{EB}$ with ΔM is shown in Fig. 10 for x = 50. The linear behavior between $H_{EB}$ and ΔM indicates that both are inter-related and have the same origin. It also implies the fact that the number of moments participating in exchange bias effect is equal to those responsible for the appearance of vertical shift in hysteresis curve.[44,47]

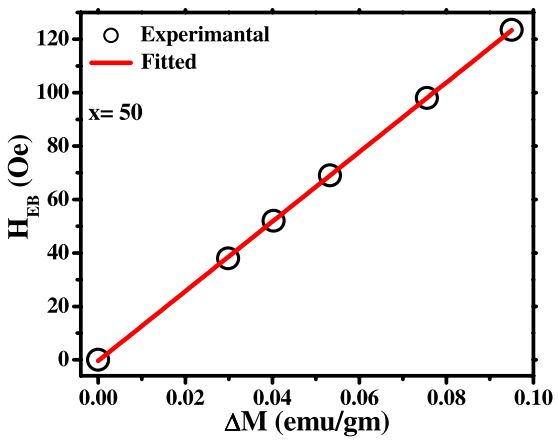


FIG. 10. $H_{EB}$ Vs ΔM for (x)$BiFeO_3$/(100 − x)NiO, x = 50.

## IV. CONCLUSION

Simple solvothermal technique has been utilized in order to synthesis BFO nanocrystals and BFO/NiO interfaces. The dispersion of BFO nanocrystals into NiO matrix leads to an enhancement of $H_{EB}$ as compared to pure NiO due to increase in exchange coupling at the interface. The maximum value of exchange field of 123.5 Oe and coercivity of 235 Oe are observed for equal concentration of BFO and NiO (50:50) in nanocomposites. The positive vertical magnetization shift for all compositions supports the existence of direct exchange interaction among pinned and uncompensated spins of NiO and BFO nanocrystals across the interface. Strong exchange coupling and discontinuity in the crystal structure across the interface lead to interesting magnetic property in the nanocomposite. Moreover, a moderate value of $H_{EB}$ and $H_C$ at room temperature makes the nanocomposite an interesting and attractive for various multifunctional nanodevices operating at room temperature.

## ACKNOWLEDGMENTS

Kaushik Chakrabarti, Babusona Sarkar, and Kajari Das are thankful to the Council of Scientific and Industrial Research (CSIR), Government of India, for providing fellowship. This work was funded by the Council of Scientific and Industrial Research, Government of India, Scheme No. 03(1210)/12/EMR-II.

[1]W. H. Meiklejohn and C. P. Bean, Phys. Rev. **102**, 1413 (1956).
[2]J. Nogues and I. K. Schuller, J. Magn. Magn. Mater. **192**, 203 (1999).
[3]M. Kiwi, J. Magn. Magn. Mater. **234**, 584 (2001).
[4]C. Chappert, A. Fert, and F. N. Van Dau, Nature Mater. **6**, 813 (2007).
[5]B. Dieny, V. S. Speriosu, S. S. P. Parkin, B. A. Gurney, D. R. Wilhoit, and D. Mauri, Phys. Rev. B **43**, 1297 (1991).
[6]T. Lin, G. L. Gormant, and C. Tsangt, IEEE Trans. Magn. **32**, 3443 (1996).
[7]V. Skumryev, S. Stoyanov, Y. Zhang, G. Hadjipanayis, D. Givord, and J. Nogues, Nature (London) **423**, 850 (2003).
[8]L. Del Bianco, D. Fiorani, A. M. Testa, E. Bonetti, and L. Signorini, Phys. Rev. B **70**, 052401 (2004).
[9]J. Nogues, J. Sort, V. Langlais, V. Skumryev, S. Surinach, J. S. Munoz, and M. D. Barob, Phys. Rep. **422**, 65 (2005).
[10]M. Ali, P. Adie, C. H. Marrows, D. Greig, B. J. Hickey, and R. L. Stamps, Nature Mater. **6**, 70 (2007).

[11]C. Cirillo, A. G. Santiago, J. M. Hernandez, C. Attanasio, and J. Tejada, J. Phys.: Condens. Matter **25**, 176001 (2013).
[12]W. Baaziz, B. P. Pichon, C. Lefevre, C. U. Bouillet, J. M. Greneche, M. Toumi, T. Mhiri, and S. B. Colin, J. Phys. Chem. C **117**, 11436 (2013).
[13]J. Sort, J. Nogues, X. Amils, S. Surinach, J. S. Munoz, and M. D. Baro, J. Magn. Magn. Mater. **219**, 53 (2000).
[14]O. Iglesias, A. Labrta, and X. Batlle, J. Nanosci. Nanotechnol. **8**, 2761 (2008).
[15]X. H. Liu, W. B. Cui, X. K. Lv, W. Liu, X. G. Zhao, D. Li, and Z. D. Zhang, J. Appl. Phys. **103**, 103906 (2008).
[16]M. Fraune, U. Rudiger, G. Guntherodt, S. Cardoso, and P. Freitas, Appl. Phys. Lett. **77**, 3815 (2000).
[17]R. H. Kodama, S. A. Makhlouf, and A. E. Berkowitz, Phys. Rev. Lett. **79**, 1393 (1997).
[18]E. Winkler, R. D. Zysler, M. V. Mansilla, D. Fiorani, D. Rinaldi, M. Vasilakaki, and K. N. Trohidou, Nanotechnology **19**, 185702 (2008).
[19]S. D. Tiwari and K. P. Rajeev, Phys. Rev. B **72**, 104433 (2005).
[20]E. Winkler, R. D. Zysler, M. V. Mansilla, and D. Fiorani, Phys. Rev. B **72**, 132409 (2005).
[21]J. Wang, J. B. Neaton, H. Zheng, V. Nagarajan, S. B. Ogale, B. Liu, D. Viehland, V. Vaithyanathan, D. G. Schlom, U. V. Waghmare, N. A. Spaldin, K. M. Rabe, M. Wuttig, and R. Ramesh, Science **299**, 1719 (2003).
[22]C. Ederer and N. A. Spaldin, Phys. Rev. B **71**, 060401 (2005).
[23]W. Eerenstein, N. D. Mathur, and J. F. Scott, Nature (London) **442**, 759 (2006).
[24]S. W. Cheong and M. Mostovoy, Nature Mater. **6**, 13 (2007).
[25]R. Ramesh and N. A. Spaldin, Nature Mater. **6**, 21 (2007).
[26]A. Singh, V. Pandey, R. K. Kotnala, and D. Pandey, Phys. Rev. Lett. **101**, 247602 (2008).
[27]F. Gao, Y. Yuan, K. F. Wang, X. Y. Chen, F. Chen, J. M. Liu, and Z. F. Ren, Appl. Phys. Lett. **89**, 102506 (2006).
[28]T. J. Park, G. C. Papaefthymiou, A. J. Viescas, A. R. Moodenbaugh, and S. S. Wong, Nano Lett. **7**, 766 (2007).
[29]L. W. Martin, Y. H. Chu, M. B. Holcomb, M. Huijben, P. Yu, S. J. Han, D. Lee, S. X. Wang, and R. Ramesh, Nano Lett. **8**, 2050 (2008).
[30]T. L. Qu, Y. G. Zhao, P. Yu, H. C. Zhao, S. Zhang, and L. F. Yang, Appl. Phys. Lett. **100**, 242410 (2012).
[31]L. W. Martin, Y. H. Chu, Q. Zhan, R. Ramesh, S. J. Han, S. X. Wang, M. Warusawithana, and D. G. Schlom, Appl. Phys. Lett. **91**, 172513 (2007).
[32]P. K. Manna, S. M. Yusuf, R. Shukla, and A. K. Tyagi, Phys. Rev. B **83**, 184412 (2011).
[33]S. Dong, Y. Yao, Y. Hou, Y. Liu, Y. Tang, and X. Li, Nanotechnology **22**, 385701 (2011).
[34]A. Querejeta-Fernandez, M. Parras, A. Varela, F. D. Monte, M. Garcia-Hernandez, and J. M. Gonzalez-Calbet, Chem. Mater. **22**, 6529 (2010).
[35]S. Larumbe, J. I. Perez-Landazabal, J. M. Pastor, and C. G. Polo, J. Appl. Phys. **111**, 103911 (2012).
[36]R. T. Lechner, G. Springholz, M. Hassan, H. Groiss, R. Kirchschlager, J. Stangl, N. Hrauda, and G. Bauer, Appl. Phys. Lett. **97**, 023101 (2010).
[37]W. Z. Ostwald, Phys. Chem. **22**, 289 (1897).
[38]G. S. Illia, M. Jobbagy, A. Regazzoni, and M. Blesa, Chem. Mater. **11**, 3140 (1999).
[39]F. B. Lewis and N. H. Saunders, J. Phys. C: Solid State Phys. **6**, 2525 (1973).
[40]T. R. Paudel, S. S. Jaswal, and E. Y. Tsymbal, Phys. Rev. B **85**, 104409 (2012).
[41]C. Ederer and N. A. Spaldin, Phys. Rev. B **71**, 224103 (2005).
[42]J. B. Quiquia, A. Lessig, A. Ballestar, C. Zandalazini, G. Bridoux, F. Bern, and P. Esquinazi, J. Phys.: Condens. Matter **24**, 366006 (2012).
[43]J. Nogues, C. Leighton, and I. K. Schuller, Phys. Rev. B **61**, 1315 (2000).
[44]Z. M. Tian, S. L. Yuan, L. Liu, S. Y. Yin, L. C. Jia, P. Li, S. X. Huo, and J. Q. Li, J. Phys. D: Appl. Phys. **42**, 035008 (2009).
[45]J. H. He, S. L. Yuan, Y. S. Yin, Z. M. Tian, P. Li, Y. Q. Wang, K. L. Liu, and C. H. Wang, J. Appl. Phys. **103**, 023906 (2008).
[46]Y. K. Tang, Y. Sun, and Z. H. Cheng, Phys. Rev. B **73**, 174419 (2006).
[47]Z. M. Tian, S. L. Yuan, S. Y. Yin, L. Liu, J. H. He, H. N. Duan, P. Li, and C. H. Wang, Appl. Phys. Lett. **93**, 222505 (2008).
[48]M. D. Stiles and R. D. McMichael, Phys. Rev. B **60**, 12950 (1999).
[49]M. D. Stiles and R. D. McMichael, Phys. Rev. B **59**, 3722 (1999).
[50]S. Sahoo, S. Polisetty, Y. Wang, T. Mukherjee, X. He, S. S. Jaswal, and C. Binek, J. Phys.: Condens. Matter **24**, 096002 (2012).
[51]V. I. Nikitenko, V. S. Gornakov, L. M. Dedukh, Yu. P. Kabanov, A. F. Khapikov, A. J. Shapiro, R. D. Shull, A. Chaiken, and R. P. Michel, Phys. Rev. B **57**, R8111 (1998).
[52]J. Wang, W. N. Wang, X. Chen, H. W. Zhao, J. G. Zhao, and W. Sh. Zhan, Appl. Phys. Lett. **77**, 2731 (2000).